ISSN 1674-1056
http://cpb.iphy.ac.cn
http://iopscience.iop.org/cpb
中国物理 B
Chinese Physics
中国物理
Chinese Physics B

Recent research process on perovskite photodetectors:A review for photodetector–materials, physics, and applications

Yan Zhao(赵岩), Chenglong Li(李成龙), Liang Shen(沈亮)

Citation: Chin. Phys. B . 2018, 27(12): 127806. **doi:** 10.1088/1674-1056/27/12/127806
Journal homepage: http://cpb.iphy.ac.cn; http://iopscience.iop.org/cpb

What follows is a list of articles you may be interested in

Studies on the polycrystalline silicon/SiO_2 stack as front surface field for IBC solar cells by two-dimensional simulations

Shuai Jiang(姜帅), Rui Jia(贾锐), Ke Tao(陶科), Caixia Hou(侯彩霞), Hengchao Sun(孙恒超), Zhiyong Yu(于志泳), Yongtao Li(李勇滔)

Chin. Phys. B . 2017, 26(8): 087802. **doi:** 10.1088/1674-1056/26/8/087802

Roles of voltage in semi-insulating GaAs photoconductive semiconductor switch

Hai-Juan Cui(崔海娟), Hong-Chun Yang(杨宏春), Jun Xu(徐军), Yu-Ming Yang(杨宇明), Zi-Xian Yang(杨子贤)

Chin. Phys. B . 2017, 26(1): 017804. **doi:** 10.1088/1674-1056/26/1/017804

Effects of oblique incidence on terahertz responses of planar split-ring resonators

Pan Xue-Cong, Xia Xiao-Xiang, Wang Li

Chin. Phys. B . 2014, 23(5): 057804. **doi:** 10.1088/1674-1056/23/5/057804

TOPICAL REVIEW — Photodetector: Materials, physics, and applications

Recent research process on perovskite photodetectors: A review for photodetector — materials, physics, and applications*

Yan Zhao(赵岩), Chenglong Li(李成龙), and Liang Shen(沈亮)†

State Key Laboratory of Integrated Optoelectronics, College of Electronic Science and Engineering, Jilin University, Changchun 130012, *China*

(Received 19 September 2018; revised manuscript received 8 October 2018; published online 25 November 2018)

The perovskite photodetectors can be used for image sensing, environmental monitoring, optical communication, and chemical/biological detection. In the recent five years, the perovskite photoelectric detectors with various devices are well-designed and have made unprecedented progress of light detection. It is necessary to emphasize the most interesting works and summarize them to provide researchers with systematic information. In this review, we report the recent progress in perovskite photodetectors, including highly sensitive, ultrafast response speed, high gain, low noise, flexibility, and narrowband, concentrating on the photodetection performance of versatile halide perovskites (organic–inorganic hybrid and all inorganic compositions). Currently, organic–inorganic hybrid and all-inorganic halide microcrystals with polycrystalline film, nanoparticle/wire/chip, and block monocrystalline morphology control show important performance in response rate, decomposition rate, noise equivalent power, linear dynamic range, and response speed. It is expected that a comprehensive compendium of the research status of perovskite photodetectors will contribute to the development of this area.

Keywords: perovskite photodetectors, response speed, detectivity, linear dynamic range

PACS: 78.56.–a, 78.66.Db, 78.66.Sq, 78.66.Tr **DOI:** 10.1088/1674-1056/27/12/127806

1. Introduction

A photodetector is a kind of device that detects and measures the characteristics of light through the photoelectric effect, and the main manifestation is photoelectric current. At present, there is growing concern about the use of photoelectric conversion techniques in detectors, including image registration, optical communication, environmental monitoring, and chemical/biological testing. Semiconductor materials must be required to absorb emitted photons and generate electron hole pairs under the light excitation, and it is also necessary to build or apply electric fields. Most photodetectors are made of inorganic semiconductors.[1] In particular, GaN^{-}-, Si^{-}-, and $InGaAs^{-}$-based photodetectors are respectively used for three important sub-bands, namely, ultraviolet (0.25 μm–0.4 μm), visible (0.45 μm–0.8 μm), and near-infrared (0.9 μm–1.7 μm). With gradual maturity of manufacturing processes and technologies of the photodetectors, their complexity, high cost, lack of mechanical flexibility, and high drive voltage have become the main disadvantages that limit their wide application and the promotion, compatibility and versatility of new technologies. In the past few years, photoelectronic materials, such as organic materials, nanomaterials, and nanocomposites, have shown great potential in simple, low-cost, flexible, and large-area photodetectors.[2–10] However, due to their poor charge-carrier characteristics, their optical detection performance has been further improved. Recently, it has been proved that the mobility of halides combined with high-charge carriers, effective light absorption, and easy-to-treat solutions are also powerful candidates for high-performance photoelectric detectors.[11,12] The development of solar cells shows that the light-emitting properties of perovskite semiconductors have been reactivated, including light-emitting diodes and lasers. Although potassium halides have the advantages of high purity and tunable bandgap, the inherent low-exciton binding can lead to a small electron pore capture rate of radiation recombination, which limits the efficient development of potassium halides.[13] Therefore, the use of ultra-thin pyroxene layers or small pyroxene grains limits electrons and holes in space and promotes bimolecular radiation recombination. Recently, the high exciton binding energy produced by self-organizing multiquantum-well structures has been proved to play a role in light-emitting applications. Recent reviews have described developments in their applications for solar cells, light-emitting, and laser devices or fully optoelectronic devices.[14] In this review, we build on the latest developments in the perovskite-based photodetector, such as responsiveness, decomposition, noise equivalent power, linear dynamic range, and response speed. Emphasis is placed on the light detection performance of multipurpose potassium halides (organic-inorganic mixtures and all inorganic components) and assembled potassium–semiconductor heterojunction materials in dual-terminal devices (photodiodes and photoconductors) and triterminal devices (photocrystals). First,

*Project supported by the International Cooperation and Exchange Project of Jilin Province, China (Grant Nos. 20170414002GH and 20180414001GH).

†Corresponding author. E-mail: shenliang@jlu.edu.cn

© 2018 Chinese Physical Society and IOP Publishing Ltd

we summarize the key performance parameters used to describe the characteristics of the photodetector. Then, according to different types of photodetectors (photodiodes, photoconductors, and photocrystals), different working mechanisms and photodetection performances of photodetectors are discussed and summarized. For photodiodes, we further investigate the performance improvement on the interface engineering. Finally, we briefly summarize the current challenges of the perovskite-based photodetector.

2. Performance parameters of photodetectors

Here, some very important performance parameters to describe the characteristics of a photodetector can be summarized as follows:

(i) **Responsivity**: The responsivity is given as the ratio of the output current or voltage to the power of the input light signal, and the unit is A/W or V/W.

(ii) **External quantum efficiency (EQE)**: EQE is the ratio of the number of charge carriers collected by photodetectors to the number of incident photons.

(iii) **Noise equivalent power (NEP)**: NEP is the signal power that produces a signal-to-noise ratio (SNR) to be equal to 1, representing the minimum impinging optical power that a photodetector can distinguish from the noise. It can be written as

$$\mathrm{NEP} = \frac{i_n}{R}. \tag{1}$$

(iv) **Linear dynamic range (LDR)**: It describes a light intensity range in which the current response of the photodetector is linearly proportional to the light intensity, and it can be calculated by

$$\mathrm{LDR} = 20\log\frac{P_{\max}}{P_{\min}}. \tag{2}$$

(v) **Response speed**: It defines the rising time (T_{R}) and falling time (T_{F}) of the optical signal reaction, which is between 10% and 90% of the maximum photocurrent.

3. Progress in the development of perovskite photodetectors

3.1. High gain

With a large optical conductivity and low noise, a higher specific detectivity can be possibly achieved. The photoelectric conduction gain is determined by calculating the ratio of the charge recombination lifetime (τ_{r}) to the charge transfer time (τ_{t}) when the transmitted charge generated by the photon can pass through the circuit several times before recombination.[15] How to design perovskite photodetectors with high gain and high performance becomes a challenge. Professor Huang and his colleagues described the manufacturing process and characteristics of the $CH_3NH_3PbI_3$ photodetector, providing a solution that combines high light conductivity from ultraviolet to infrared with wide spectral response.[16] As shown in Fig. 1(a), here is a layered inverted structure where indium tin oxide (ITO) is the cathode, $CH_3NH_3PbI_3$ is the active layer, 4,4′-bis[(p-trichlorosilylpropylphenyl)phenylamino]-biphenyl (TPD–Si_2) serves as the hole transporting/electron blocking layer, molybdenum trioxide (MoO_3) is used for anode work function modification, and silver (Ag) as the anode.

Thanks to the electron injection induced by the trap hole in the dark, the $CH_3NH_3PbI_3$ photodetector acts as a photodiode, and at the same time, the light shows a huge photoconductive gain.[17] At a very low drive voltage of -1 V, the maximum device gain is 489 ± 6. The key to achieving high gain is the porosity caused by high-density Pb^{2+} cations on the surface of the high-temperature layer. The organometal trihalide perovskites (OTP) photodetector requires very low bias pressure, and uses miniature button batteries to bind closely to the existing low voltage circuits.[18]

Professor Jiang has studied a simple method to control the growth alignment of perovskite monocrystals, and its application for high-performance photoelectric detectors has been demonstrated.[19] It provides an effective base of precise regulation of liquid position, alignment, and fluid dynamics, and ensures effective control of crystallization process.

The photodetector is made of a crystal arranged one-dimensional (1D) high temperature rock array. The following set of current–voltage (I–V) curves to depict different incident powers under the dark light are very representative, as shown in Fig. 2(a). A dark flow of 8.13×10^{-10} A is observed due to the low concentration of carriers in perovskite monocrystalline arrays. After illumination, the current increases due to the high carrier concentration of light excitation at the same time, and it shows a significant power dependence (Fig. 2(a)). For the diagonal I–V curve of 2.82 nW, the curves in the dark and under illumination show a high light closure close to 10^3, as shown in the inset of Fig. 2(a). Figure 2(b) shows the photoelectric current and response rate associated with the incident power.

Because the 1D single crystal array has the characteristics of high crystallinity and crystal sequence, high response and fast excellent performance of photoelectric detectors have been achieved. Anisotropy light absorption resulting from the strict alignment of 1D structures leads to the application of polarization sensitive light detection.

Zhang and his colleagues described a new molecular design for the production of organic photodetectors (OPDs) with unprecedented photon recognition capabilities.[20] Because inorganic materials can be used as lightweight and mechanical flexible devices, they have potential ease of use. Therefore, the use of organic materials as active ingredients in photoelectric detectors is very popular.[21]

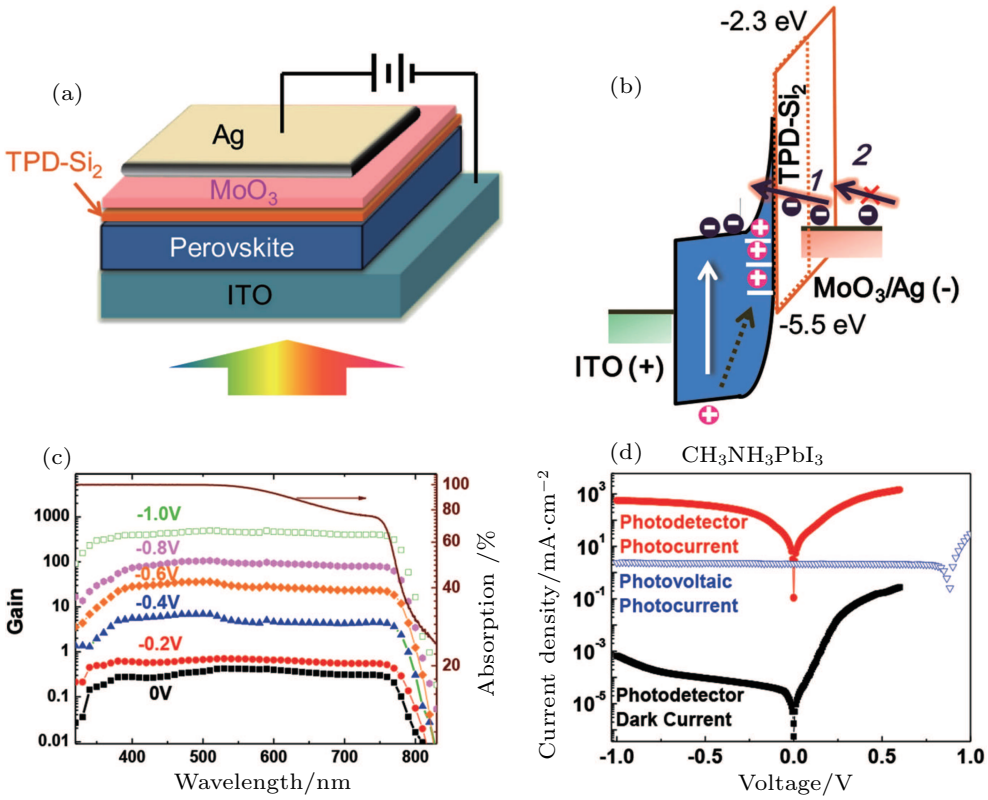


Fig. 1. (color online) (a) Device structure of the $CH_3NH_3PbI_3$ photodetector. (b) Energy diagram of the $CH_3NH_3PbI_3$ photodetector at reverse bias under illumination. (c) Absorption spectrum (solid line) of the $CH_3NH_3PbI_3$ films and wavelength-dependent gain (solid lines with symbols) of the $CH_3NH_3PbI_3$ devices under reverse biases between 0 V to −1 V. (d) Photo- and dark-current density–voltage curves of the $CH_3NH_3PbI_3$ device (from Ref. [16]).

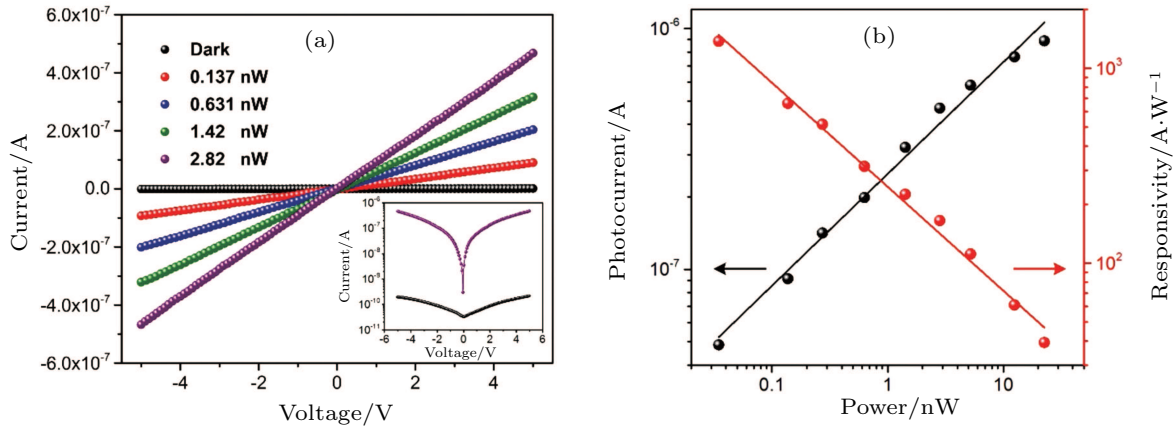


Fig. 2. (color online) Device performance of single-crystalline perovskite photodetectors. (a) Dark current and photocurrent under different illumination powers of 1D perovskite arrays. The inset shows logarithmic *I*–*V* curves in the dark and under illumination with a power of 2.82 nW. (b) Photocurrent and responsivity of device under different incident powers (from Ref. [19]).

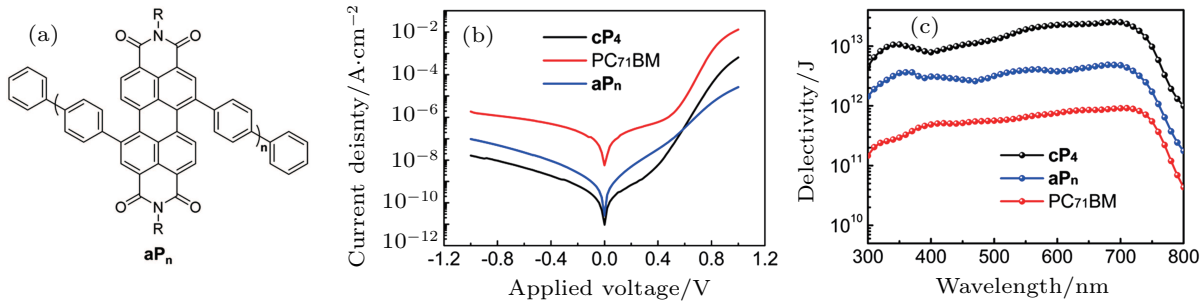


Fig. 3. (color online) (a) Molecular structure of aP_n-used to test the origin of the low dark current. (b) Dark current density–voltage curves for $PC_{71}BM$-, aP_n-, and cP_4-based photodetectors. (c) Specific detectivity spectra for cP_4-, aP_n-, and $PC_{71}BM$-based OPDs calculated at −0.1-V bias voltage (from Ref. [20]).

As shown in Fig. 3, the results show that the rigid cyclic molecular structure is a significant design criterion to realize the superconductivity of organic oxides. The authors have also found that rigid conjugated macrorings can act as electron receptors in high-performance photocells. Using this finding, they can also suppress the undercurrent density while retaining the high response to an ultra-sensitive non-fullerene OPD. Compared with the best fullerene-based photodetector, this decomposition rate can require no additional carrier blocking layer, and the sensitivity at low operating voltage is a record for non-fullerene OPDs. This study clearly shows that the designed electronic materials can shape and match these macrocyclic electron receptors, thus further improving the performance of the device.

3.2. Low noise

Low noise limits the sensitivity of the perovskite photodetector. Therefore, how to design a low-noise perovskite photodetector came into being. In view of the development of organic semiconductor based photodetectors, photodiodes that follow the solar cell structure generally show lower noise and faster response speed. In order to obtain low noise and fast response perovskite photodiodes, research groups employed the planar solar cell architecture to the effect of mesoporous layer on dark current and response speed should not appear as much as possible.

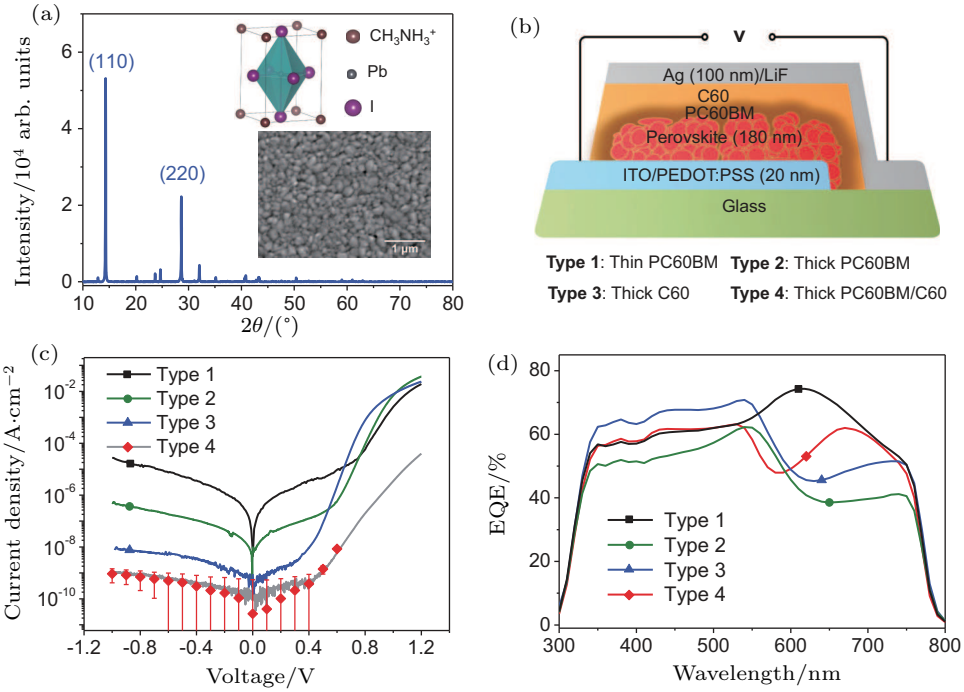


Fig. 4. (color online) (a) X-ray diffraction (XRD) pattern of solution processed perovskite films on ITO/PEDOT:PSS with the crystal structure pictured in the inset. (b) Cartoon of the four different perovskite photodiode (PPD) structures: Type 1 with thin $PC_{60}BM$ (10 nm) layer, Type 2 with thick $PC_{60}BM$ (50 nm) layer, Type 3 with thick C_{60} layer, and Type 4 with thick $PC_{60}BM$ (50 nm)/C_{60} (130 nm) layer. (c) Dark current density–voltage (J–V) characteristics obtained at a scanning rate of 1 mV·s^{-1}. Each point shown for the Type 4 devices are an average of the dark current measured over several seconds after each voltage step. (d) Typical external quantum efficiency spectra (measured at 120 Hz) for each of the four PPD types (from Ref. [22]).

Lin *et al.* used the thicker C_{60} and [6,6]-phenyl-C_{61}-butyric acid methyl ester ($PC_{60}BM$) difuller layer to replace the poly[(9,9-bis(3′-(*N*, *N*-dimethylamino)propyl)-2,7-fluorene)-alt-2,7-(9,9-dioctylfluorene)] (PFN), which becomes a porous blocking layer to manufacture perovskite photodetectors (See Fig. 4).[22] The C_{60} cathode interlayer has the following advantages: (i) The so-called a relatively easy analytical homotopy covered by the C_{60}/$PC_{60}BM$ cathode sandwich forms the perovskite photodiode. Its performance is a low shunt capacitor that improves the time response to the diodes; (ii) it inhibits the dark current and limits the return hole through a conformal coating into the homotopy junction of the high temperature layer; (iii) the electro–optical control that provides the spectral response is achieved without damaging the LDR, as the migration of fullerene electrons is sufficient to prevent the formation of a space charge at the junction where the light intensity is as high as 0.4 W/cm^2. The measured LDR the authors observed was 170 dB (at −0.5 V), but the noise calculation indicated that it may reach 250 dB. This work further proves the great potential for organic halides in optoelectronics and provides a related silicon substitution technology for visible light detection and imaging.[23]

Simultaneously, Fang *et al.* used a thick C_{60}/PCBM fullerene double layer as a hole blocking layer to cut down the leakage current and capacitance of the device, thereby increasing the reaction speeds.[24] As shown in Fig. 5, the device is able to directly measure the intensity of visible light from 1 mW·cm^{-2} to sub 1 pW·cm^{-2}.

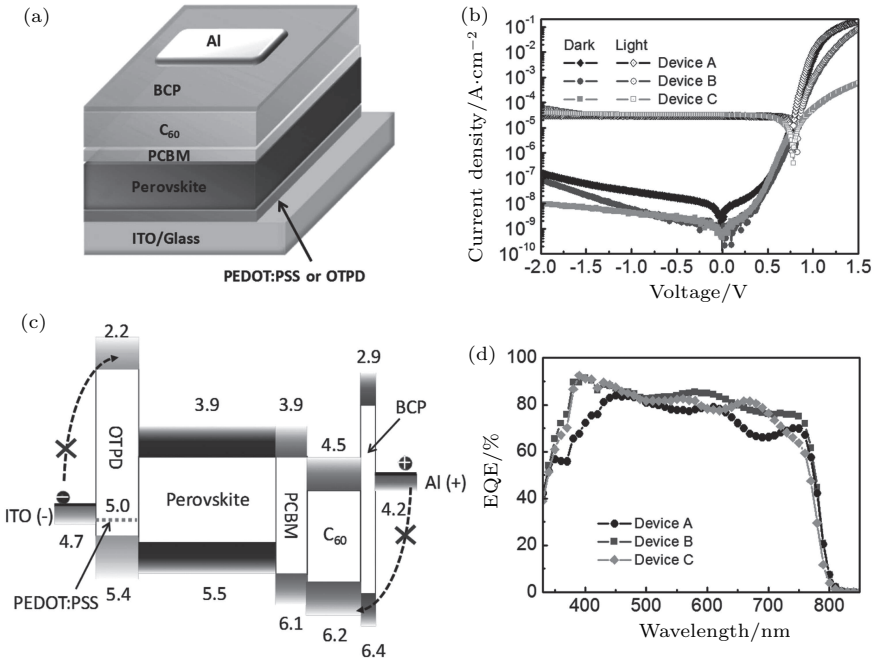


Fig. 5. (a) The schematic device structure of perovskite photodetectors. (b) The dark current (solid symbols) and photocurrent density (hollow symbols, under white light ≈ 143 μW·cm^{-2}) *versus* bias curves of devices A (diamonds), B (circles), and C (squares). (c) The energy diagram of the perovskite photodetectors. (d) The EQE curves of devices A (circles), B (squares), and C (diamonds) at −0.1 V with the incident light modulation frequency of 35 Hz (from Ref. [24]).

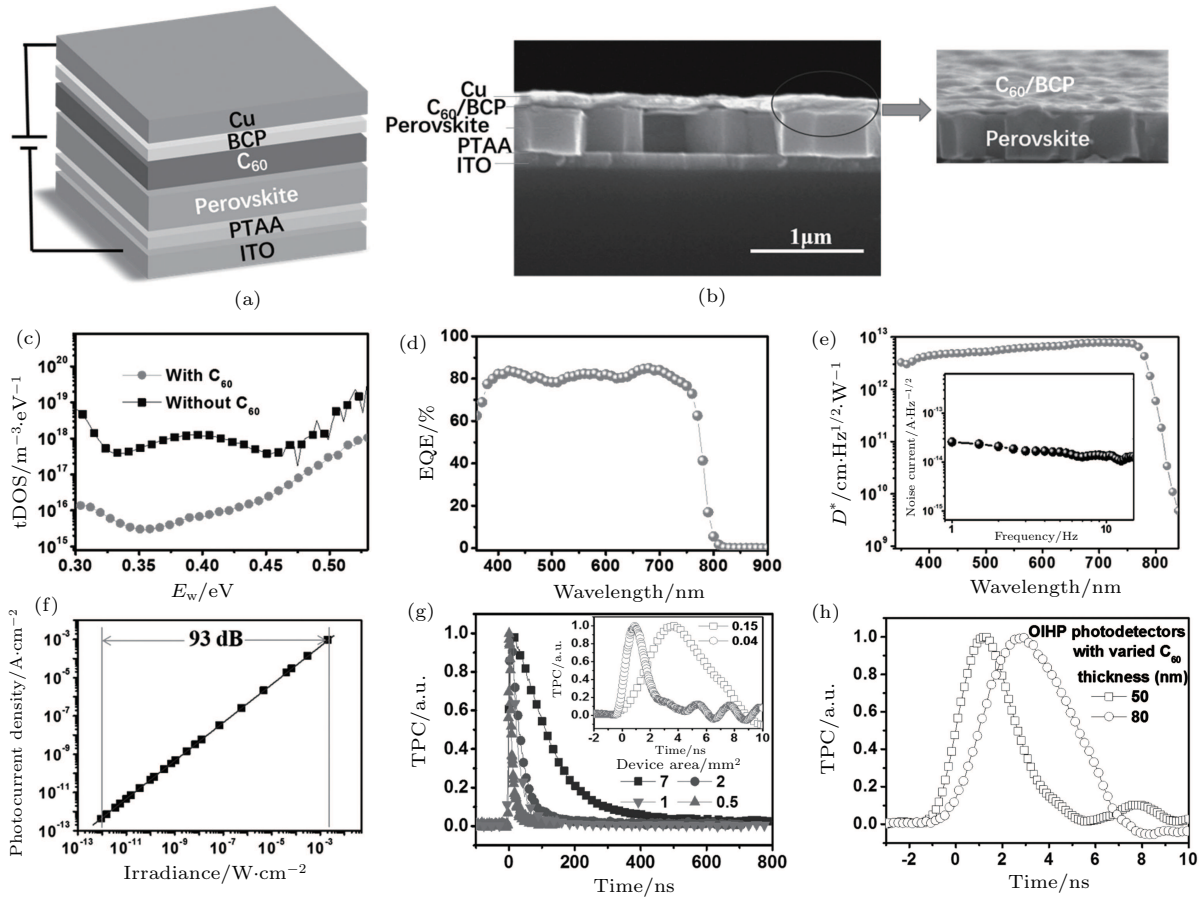


Fig. 6. (a) Schematic device structure of the OIHP photodetectors. (b) Cross-section scanning electron microscope (SEM) image of an OIHP photodetector. Inset: a tilted view of perovskite and C_{60}/2,9-dimethyl-4,7-diphenyl-1,10-phenanthroline (BCP) layer. (c) The trap density of states curve *versus* demarcation energy with or without C_{60} in the devices. (d) EQE of the OIHP photodetector at zero bias. (e) The specific detectivity of the OIHP photodetector at different light wavelengths under −0.1-V bias voltage. Inset: The noise current of the OIHP photodetector at −0.1 V. (f) The linear dynamic range of the OIHP photodetector under an LED illumination of various light intensities. The solid line represents linear fitting to the data. (g) The transient photocurrent (TPC) curves of the devices with different areas from 7 mm^2 down to 0.04 mm^2. TPC lifetime: 115.1 ns for 7 mm^2; 35.3 ns for 2 mm^2; 17.9 ns for 1 mm^2; and 9.0 ns for 0.5 mm^2. Inset: 2.7 ns for 0.15 mm^2; 1.0 ns for 0.04 mm^2. (h) TPC curves of the perovskite photodetectors with different C_{60} thicknesses. TPC lifetime: 1.4 ns for 50 nm and 2.5 ns for 80 nm (from Ref. [25]).

In general, the highly sensitive perovskite photodetector described here has low noise (16 fA·Hz$^{-1/2}$, at −0.1 V) close to the limit of shot and thermal noise, with a high average equivalent of about 90%, a large LDR of 94 dB, and a reduced response time of 120 ns. The interface design and hole transport layers (HTLs) engineering, in particular, the more fully layered trap passivation effect, enable it to directly measure the irradiance of light below 1 pW·cm^{-2}, consistent with the calculated results. The photodetector has excellent weak light sensitivity and may replace commercial Si photodiodes in areas such as communications, defense, and imaging.

3.3. Fast response speed

Professor Huang and his colleagues first increased the response speed of the perovskite photodetector to 120 ns, suggesting that the perovskite photodetector can achieve ultrafast response by reducing the resistor–capacitor (RC) time constant and charge to transfer time. Shen group proposed a solvable analytic hierarchy process (AHP) photodetector with a super-fast response time of 1 ns operating in zero-bias conditions.[25,26] As shown in Fig. 6, the OIHP photodetector electron extraction layer was changed to C_{60} only to enhance its response speed, because the high mobility of C_{60}. The authors mentioned the use of these low-cost photodetectors, establishing a time resolved photoluminescence (TRPL) system, and successfully measured the radiation recombination lifetime of various optoelectronic materials between a few nanoseconds and microseconds. The authors believed that this was the first time that low-cost resolved photodetectors could meet the application requirements of high performance scientific equipment. Furthermore, they believed that these clipping photodetectors would soon be used in consumer electric because they had the best visible light imaging absorption spectrum, the rapid response speed of fast frame rate image, and the array of existing printing technique.[27,28]

Sub-nanosecond response is a significant advance to perovskite photodetectors. But, their spectral response has been limited to the UV-visible range below 800 nm. On the contrary, the solution-processable, polymer-based photodetectors have obtained spectral response of a wider range of spectral responses ranging from ultraviolet to near infrared (NIR). However, its shortcoming is slow response. In order to address the above problems, Shen *et al.* by integrating high-temperature stones while turning the polymer bulk heterojunction (BHJ) into a device, a low-noise photodetector is created that shows an ultra-fast response to ultraviolet-near infrared (UV-NIR) light.[29] The mixture device showed an external quantum efficiency of 58%–63% in the wavelength range of 340 nm to 790 nm, and 13%–19% in the wavelength range of 810 nm to 930 nm. (See Fig. 7) In addition, for exploration of the northern lights, the perovskite layer acts as an integral level, reducing the device capacitance, expanding the distance between the two electrodes, and reducing the device response time to 5 ns. This should be the fastest polymer-based photodetector to test the equipment area.

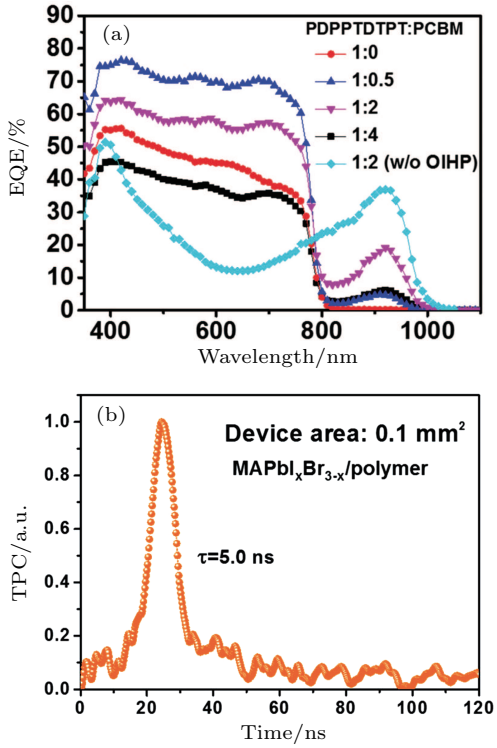


Fig. 7. (color online) (a) The EQE values of perovskite/polymer hybrid photodetectors with different poly{2,5-bis(2-hexyldecyl)-2,5-dihydropyrrolo[3,4-*c*]pyrrole-1,4-dione-3,6-di(5-thiophen-2-yl) yl-alt-*N*-(2-ethylhexyl)-dithieno-[3,2-*b*:2,3-*d*]pyrrole-2,6-diyl} (PDPPT-DTPT): PCBM ratios, and that of the pure polymer (w/o OIHP) photodetector, at a bias of −0.2 V. (b) TPC curve of the MAPbI$_x$Br$_{3-x}$/polymer hybrid photodetector with a device area of 0.1 mm^2. The TPC lifetime of the device was found to be 5.0 ns (from Ref. [26]).

3.4. Narrow band

Under certain circumstances, the specific detection is required for different wavelengths of light, so the narrowband photodetectors are really indispensable in many applications, such as video, machine vision, and optical filters.

Lin and colleagues have reported the narrowband red, green, and blue photodiodes with a full width at half maximum (FWHM) less than 100 nm. Subsequently, several significant designs appeared in succession about the charge collection narrowing (CCN) concept in organic halides, or mixed lead halides semiconductors.[30] Two absorption points were selected among them, and the authors changed the ratio of halogenated compounds in semiconductors and/or add organic (macro) molecules to the films for the composite engineering. Figure 8(a) presents optical field distributions in the red narrowband photodiodes for junction photodiode (500 nm) for four wavelengths: 350 nm, 450 nm, and 550 nm in the Beer–Lambert regime and 650 nm in the cavity regime. Figure 8(b) shows EQEs with different junction thicknesses at −0.5 V. According to the above description, the optical and electrical transmission characteristics of photodiodes could be precisely controlled, so the photodetectors cover the full vis-

ible spectrum and enter NIR with an adjustable narrowband response.[31]

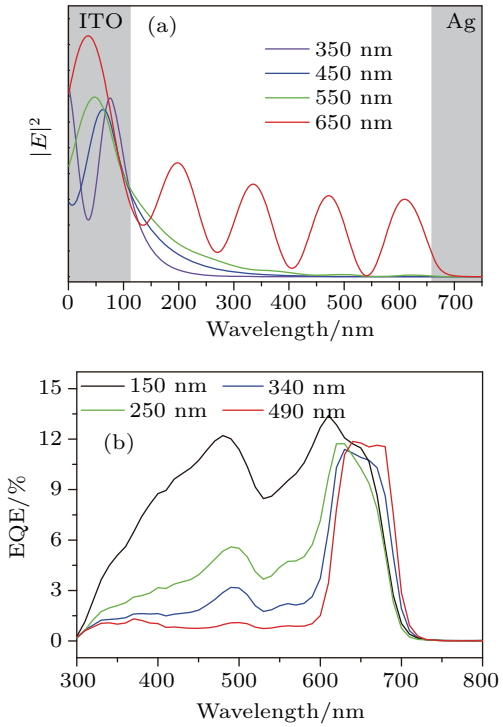


Fig. 8. (color online) (a) Optical field distributions in the red narrowband photodiodes (fidi thicknesses of 500-nm $CH_3NH_3PbI_2Br$ and 60-nm C_{60}) for four wavelengths: for $\lambda < 600$ nm (the Beer–Lambert region) photons cannot penetrate the whole of the film and carriers are surface generated, and for 700 nm$> \lambda > 600$ nm (the cavity region) the photo carriers are volume-generated. (b) EQEs of narrowband red CCN photodiodes with various junction thicknesses at a reverse bias of -0.5 V. The thinnest junction delivers an almost broadband response because surface- and volume-generated carriers are collected. By increasing the junction thickness, surface generation and volume generation are distinguished and the EQE at shorter wavelengths (in the Beer–Lambert region) is suppressed (from Ref. [30]).

The blue, green, and red photodiodes have different applications due to the individual characteristics; in addition, the most advanced narrowband performance indicators should be a low dark current, a high frequency detection rate, the large LDRs, and a fast frequency response. These performance indicators may be time-span rather than finite in practical applications. Crucially, all photodiodes are highly discretionary when designing windows with a mutative brightness. This is significant for more pure light-independent color recognition and contrast. The author's findings further demonstrate the possibility of organic halides and relevant materials for the cheap, conducive manufacturing, new generation photodetectors. The strategies above can facilitate the solution processing of different device fabrication and the actual evaporation of a variety of semiconductor applications.

In contrast, Fang and his colleagues focused on single crystals perovskite photodetectors. They have reported the growth of perovskite single crystals with monohalides, and obtained a border absorption of $MAPbBr_{3-x}Cl_x$ and $MAPbI_{3-x}Br_x$ from blue to red.[32] As shown in Fig. 9(b), these single crystal-based perovskite photodetectors show different EQE peak and tunable narrowband response. In addition, this single crystal is used as a photoactive material in the photodetectors to realize the narrow band light detection from blue to red with adjustable spectral response. To assess the capability of the narrowband photodetectors, a MAPbBr3 single crystal (1.2 mm) was used to measure narrowband photodetectors device performance (See Fig. 10).

According to the above principle, they turned the composition of the halide in the single crystal to achieve continuous modulation of the reaction spectrum in the visible scope. By comparing the results of device modeling with the measured EQE spectrum, the results of short-wave excitation inhibition charge collection caused by surface charge recombination are obtained, leading to a narrow band light detection. The FWHM is smaller than 20 nm, the rejection rate is larger than 200 from resonance, and the detection limit is 80 pW·cm^{-2}, with ultra-narrow EQE peak and high sensitivity. In addition, in order to further ameliorate the performance of the device, a gain mechanism is used to improve the responsiveness of the device and suppress the noise through buffer engineering. At the same time, both methods have been proved to significantly improve the sensitivity of the perovskite detector. In general, the recent design paradigm proposed in this work provides a substitute method for non-optical ultraviolet, visible, and infrared narrowband light detection.[33]

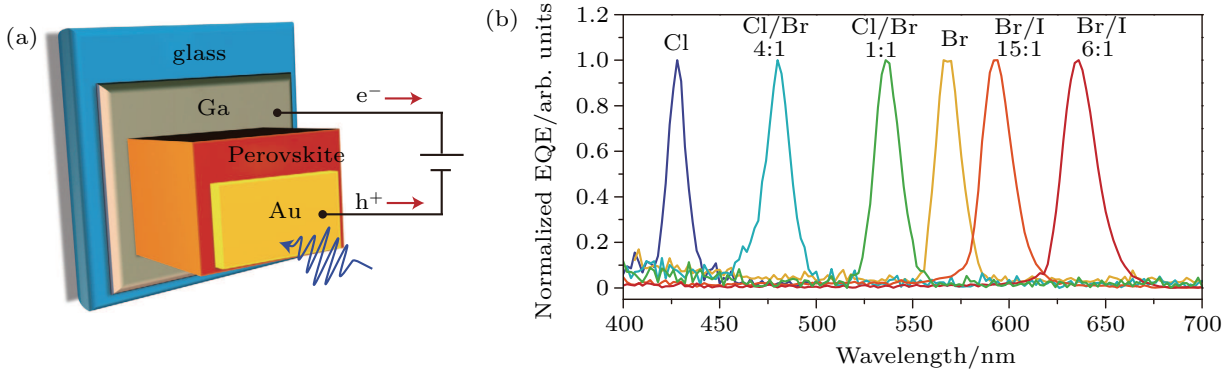


Fig. 9. (color online) (a) Schematic diagram of device structure. (b) Normalized EQE spectra of the single-halide and mixed-halide perovskite single-crystal photodetectors with different halide compositions, showing the ultra-narrow EQE peak and tunable spectral response. The EQE spectra were measured under -1-V bias (from Ref. [32]).

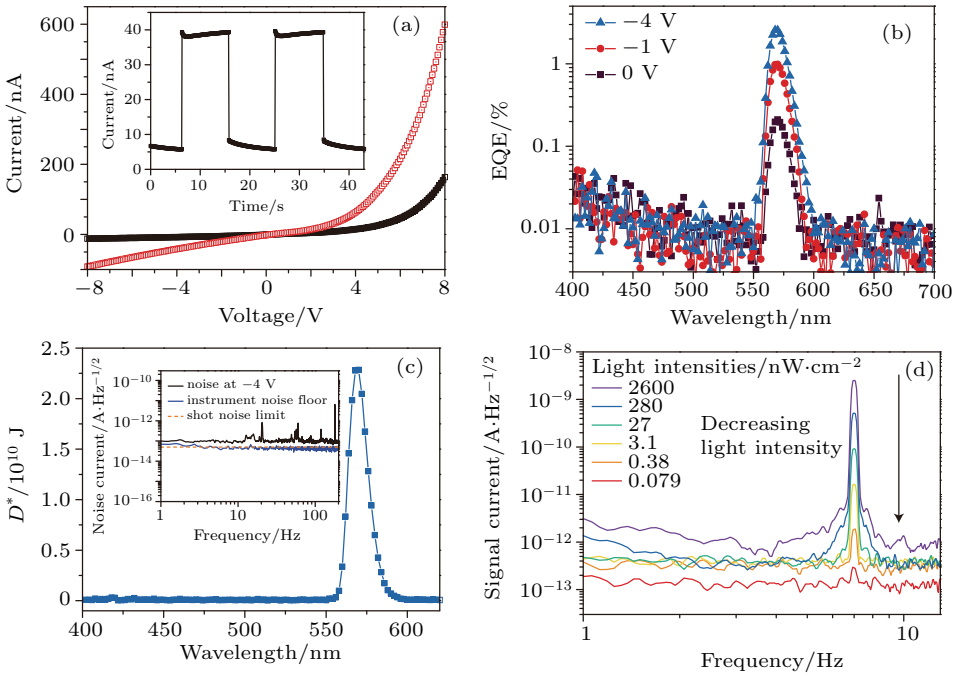


Fig. 10. (color online) (a) Dark current and photocurrent of a 1.2-mm-thick $MAPbBr_3$ single-crystal photodetector under white-light illumination of 0.4 mW·cm^{-2}. Inset: repeated operation of the photodetector in the dark and under illumination of 0.4 mW·cm^{-2} with a bias of −4 V. (b) EQE spectra under biases of 0, −1, and −4 V. (c) Specific detectivity (D^*) spectrum under −4-V bias. Inset: measured total noise under −4 V (black solid line), calculated shot noise limit (orange dashed line) and instrument noise floor (blue solid line). (d) Current spectrum under 570-nm LED illumination of different light intensities with a modulation frequency of 7 Hz for NEP measurement (from Ref. [32]).

3.5. Flexible

Compared with traditional hard silicon substrate devices, flexible photodetector has a wide range of applications in wearable and portable devices owing to its reduced cost and weight. Generally, perovskites are synthesized by solution process, which in turn can be assembled into lightweight flexible photodetectors.[34,35]

Xie and colleagues reported the first flexible perovskite photodetector in a simple ejection process on the ITO/polyethylene terephthalic acid (PET) substrate.[36] The flexible device has outstanding flexibility and robustness. Even if it bends 120 cycles, the photocurrent cannot be changed significantly. As shown in Fig. 11, carbon cloth served as served as both a contact electrode and a flexible substrate in the flexible perovskite photodetector. Furthermore, it not only exhibited wide photoresponse spectrum range but also excellent stability. The perovskite nanowire network with an ordered Au electrode template is placed by Songs and colleagues on the PET substrate. Because the new network structure, photodetector array can release a part of bending stress and the flexibility is improved. After 1000 different angles of photocurrent evolution spectrum, the response signal is almost unchanged at a fixed angle of less than 60°. At a large angle of 80°, only 20% of photocurrent can be observed. In addition, the photocurrent shrinks less than 10% after ten thousand bending cycles, showing an excellent flexibility.

What is more, Yang and his colleagues have developed a rolling micro gravure printing method for large-scale production of highly oriented and extra long $MAPbI_3$ array thin films on diverse substrates. They used this method to demonstrate the flexible device on the PET substrate, according to the performance of the medium in a recent study. They have developed a high performance on carbon cloth perovskite photodetectors in the device; carbon cloth is a substitute for traditional PET substrate, due to its excellent conductivity and better mechanical flexibility, as well as contact electrode and the flexible substrate. The device has a broad spectrum, from ultraviolet to infrared spectrum with good stability.[37]

Flexible perovskite photodetector was prepared on flexible PET substrate or carbon cloth, which is proved to have the best stability and mechanical flexibility, paving the way to the examples of portable wearable optoelectronic devices. The high-performance photodetectors handled by solution was described by Bao and his colleagues.[38] In general, traditional inorganic semiconductors are increasingly replaced by organic semiconductor materials and quantum dots, thus they can be adapted to new light detection applications, such as plastic substrates, flexible, lightweight imagers. The vectors of these solutions are fluid treatment materials, so their response speed is always low even with a high sensitivity. Recently, they have implemented the response time of the high-speed hyperlight photodetector, which was nanosecond by unbinding the RC constant of the device.

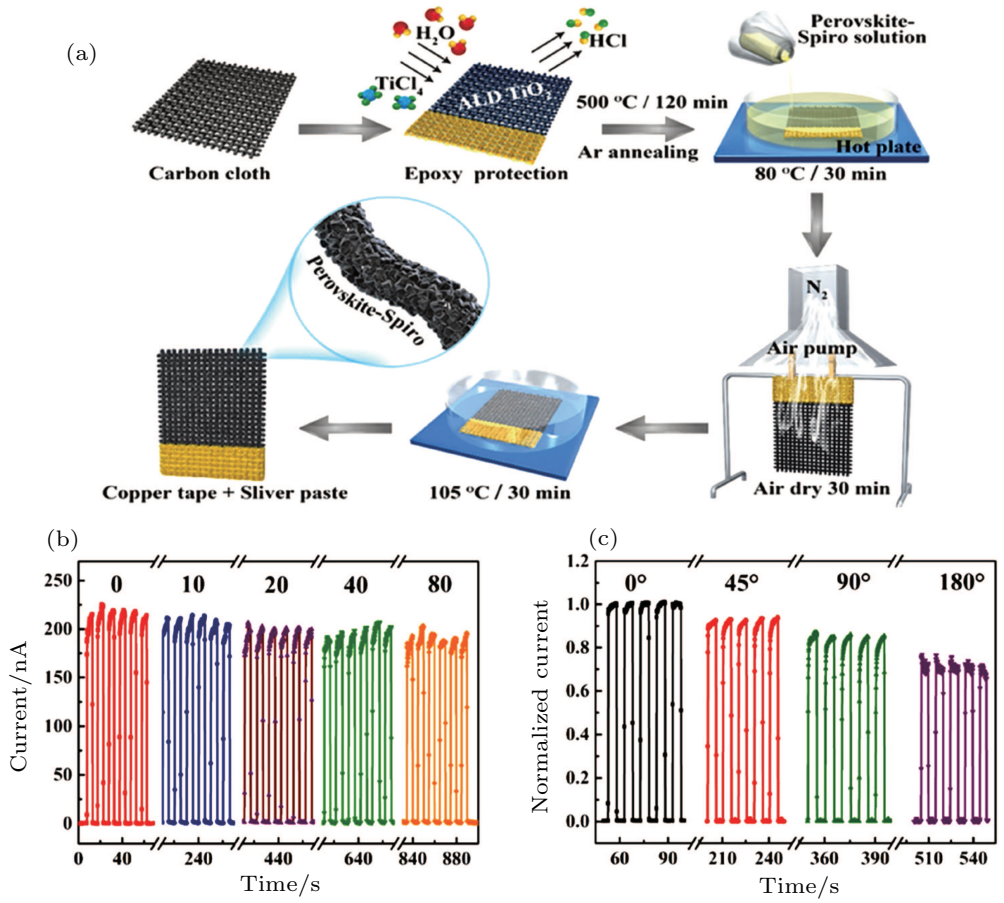


Fig. 11. (color online) (a) Fabrication process of a flexible perovskite photosensor on carbon cloth. (b) Device photoresponse after different bending cycles. (c) Normalized photoresponse curve at different bending angles. Reproduced with permission from Ref. [36].

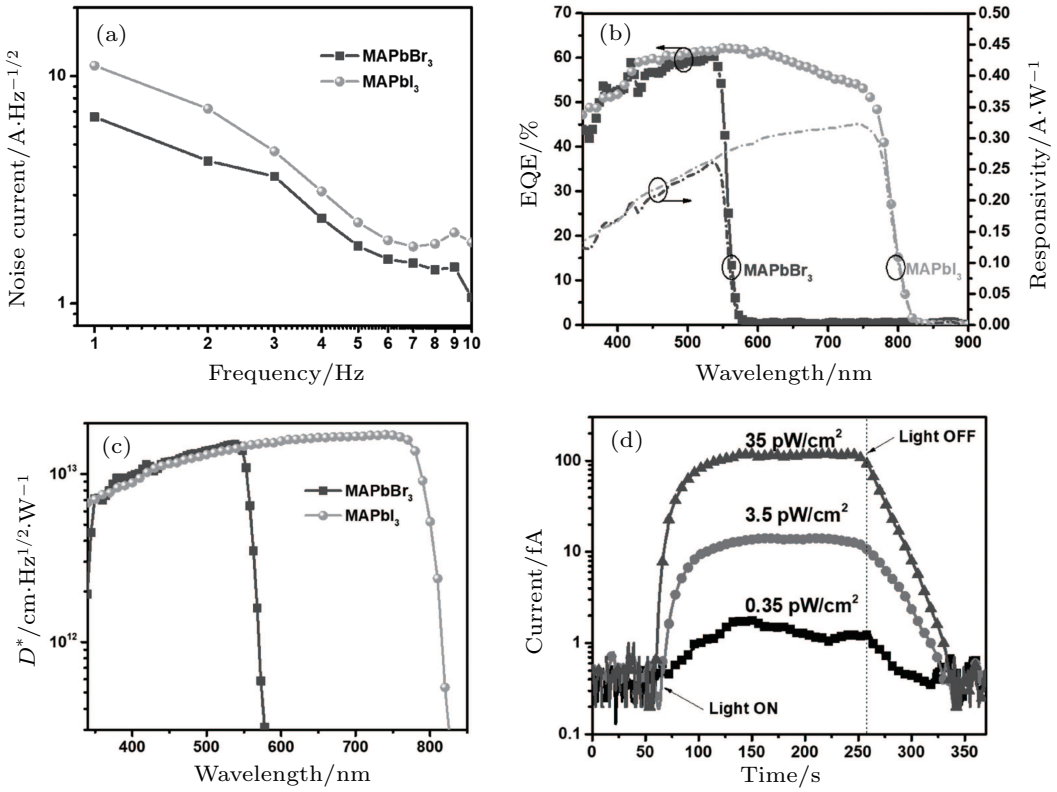


Fig. 12. (a) Noise current of photodetectors based on $MAPbBr_3$ and $MAPbI_3$ TSCs at 0-V bias voltage. (b) External quantum efficiency (EQE) and responsivity spectra of photodetectors based on $MAPbBr_3$ and $MAPbI_3$ TSCs. (c) Specific detectivity (D^*) of devices based on $MAPbBr_3$ and $MAPbI_3$ TSCs measured at 0-V bias and 8 Hz. (d) The current output of the $MAPbBr_3$ TSC device to green light with intensities of 0.35, 3.5, and 35 pW·cm^{-2} (from Ref. [38]).

The performance of p–i–n photodetector on account of austenitic single crystals (TSCs) is demonstrated in this paper. The organic–inorganic halide perovskite (OIHP) TSCs, which can grow horizontally up to millimetres in size and up to a few tens of microns in thickness, growing directly on the substrate covering the defective blunt hole transport layer. The TSCs have longer carrier recombination life and lower trapping density, while the polycrystalline film does not. The reason is that TSCs photodetectors display an ultra-low dark current, and the noise equivalent power (NEP) has dropped to a much low level. These photodetectors performance parameters of noise spectra, EQE, specific detectivity and response speed are shown in Fig. 12. In addition, as shown in Fig.13, the linear dynamic range of the $MAPbBr_3$ monocrystalline photodetector reached 256 dB because the recombinant one life of monocrystal device in bright light is much longer.[39] The author's research shows the potential of the perovskite an cornerstone monocrystals for high-performance photodetector.

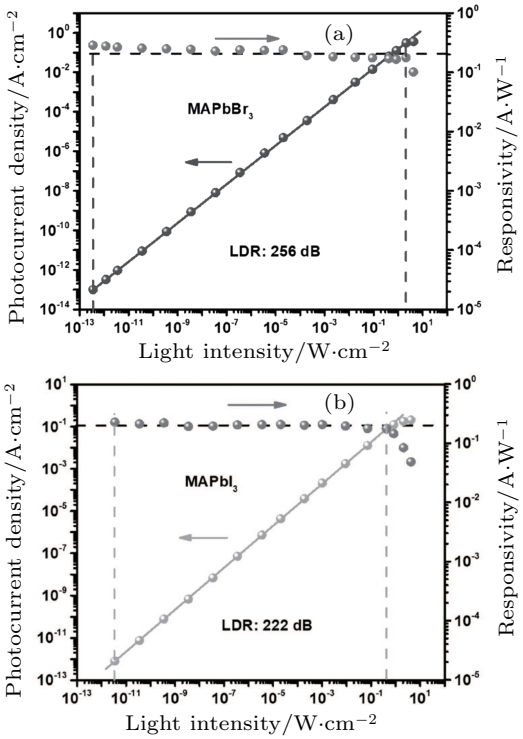


Fig. 13. The dynamic-range characterization of photodetectors based on (a) $MAPbBr_3$ and (b) $MAPbI_3$ TSCs at 0 V with green-light illumination of various light intensities. The solid line is a linear fitting to the data. The corresponding responsivity is shown in the figures with *Y* axis on the right (from Ref. [38])

4. Conclusion

Calcium–titanium-type photodetectors have made great progress in the past eight years. In terms of commercialization, perovskite photodetectors will face many challenges: the EQE, detection capabilities, flexibility, sensitivity issues, and competition from more mature competitive technologies. In order to improve responsiveness and EQE, we are committed to designing single crystals, low-dimensional nanostructures, heterojunction through integration with two-dimensional (2D) grapheme, and transition-metal dichalcogenides (TMDs). In particular, the preparation of one-dimensional nanometer/microfilament arrays rather than disordered nanowires, is a successful strategy for achieving high responsiveness. In order to reduce the dark current and increase the detection capability, especially the extremely weak light, we introduce the buffer into the photodiode by deliberately changing the electron transport layer (ETL) and hole transport layer (HTL) materials. Flexibility calcare–titanium-type photodetectors were prepared on a flexible PET substrate or carbon cloth, which proved their best stability and mechanical flexibility, paving the way to the examples of portable wearable optoelectronic devices.

The currently developed halide perovskite has a weak sensitivity to NIR light. Narrow band gap conjugated polymers or PbS quantum dots have been combined into perovskite to enhance the absorption of near-infrared regions. Our recent research has shown that upconversion nanocrystals could absorb low-energy photons and convert them up into high-energy photons, and then transfer energy to a visible light absorption semiconductor material with a matching band gap, which can be a candidate for the binding. Photosensitivity of austenitic enhanced near infrared induced charge.

References

[1] Xing G, Mathews N, Sun S, Lim S S, Lam Y M, Grätzel M, Mhaisalkar S and Sum T C 2013 *Science* **342** 344
[2] Shen L, Fang Y, Dong Q, Xiao Z and Huang J S 2015 *Appl. Phys. Lett.* **106** 023301
[3] Wei H, Fang Y, Yuan Y, Shen L and Huang J S 2015 *Adv. Mater.* **27** 4975
[4] Shen L, Fang Y, Wei H, Yuan Y and Huang J S 2016 *Adv. Mater.* **28** 2043
[5] Lee Y, Kwon J, Hwang E, Ra C H, Yoo W J, Ahn J H, Park J H and Cho J H 2015 *Adv. Mater.* **27** 41
[6] Dong Y Y, Zhao Y Z, Zhang S Y, Dai Y, Liu L, Li Y J and Chen Q 2018 *J. Mater. Chem. A* **6** 21729
[7] Dong H, Zhu H, Meng Q, Gong X and Hu W 2012 *Chem. Soc. Rev.* **41** 1754
[8] Wang W B, Du M D, Zhang M, Miao J L, Fang Y and Zhang F J 2018 *Adv. Opt. Mater.* **6** 1800249
[9] Xue D J, Shi H J and Tang J 2015 *Acta Phys. Sin.* **64** 038406 (in Chinese)
[10] Jiang S, Jia R, Tao K, Hou C X, Sun H C, Yu Z Y and Li Y T 2017 *Chin. Phys. B* **26** 087802
[11] Zhang L, Yang T, Shen L, Fang Y, Dang L, Zhou N, Guo X, Hong Z, Yang Y, Wu H, Huang J and Liang Y 2015 *Adv. Mater.* **27** 6496
[12] Wei H, Tang Y, Feng B and You H 2017 *Chin. Phys. B* **26** 128801
[13] Merabet B, Alamri H, Djermouni M, Zaoui A, Kacimi S, Boukortt A and Bejar M 2017 *Chin. Phys. Lett.* **34** 016101
[14] Xiang F, Li B Y, Li Y F, Zhou J and Gan W P 2016 *Chin. Phys. B* **25** 078110
[15] Dong R, Bi C, Dong Q, Guo F, Yuan Y, Fang Y, Xiao Z and Huang J 2014 *Adv. Mater.* **2** 549
[16] Dong R, Fang Y, Chae J, Dai J, Xiao Z, Dong Q, Yuan Y, Centrone A, Zeng X C, Huang J 2015 *Adv. Mater.* **27** 1912
[17] Gao L, Zeng K, Guo J, Ge C, Du J, Zhao Y, Chen C, Deng H, He Y, Song H, Niu G and Tang J 2016 *Nano Lett.* **16** 7446
[18] Cui H J, Yang H C, Xu J, Yang Y M and Yang Z X 2017 *Chin. Phys. B* **26** 017804
[19] Feng J, Yan X, Liu Y, Gao H, Wu Y, Su B and Jiang L 2017 *Adv. Mater.* **29** 1605993

[20] Zhang B, Trinh M T, Fowler B, Ball M, Xu Q, Ng F, Steigerwald M L, Zhu X Y, Nuckolls C and Zhong Y 2016 *J. Am. Chem. Soc.* **138** 16426
[21] Feng W, Qin C, Shen Y, Li Y, Luo W, An H and Feng Y 2015 *Sci. Rep.* **4** 3777
[22] Lin Q, Armin A, Lyons D M, Burn P L and Meredith P 2015 *Adv. Mater.* **27** 2060
[23] Xiong S, Li L, Qin F, Mao L, Luo B, Jiang Y, Li Z, Huang J and Zhou Y 2017 *ACS Appl. Mater. Interfaces* **9** 9176
[24] Fang Y and Huang J 2015 *Adv. Mater.* **27** 2804
[25] Shen L, Fang Y, Wang D, Bai Y, Deng Y, Wang M, Lu Y and Huang J 2016 *Adv. Mater.* **28** 10794
[26] Shen L, Lin Y, Bao C, Bai Y, Deng Y, Wang M, Li T, Lu Y, Gruverman A, Li W and Huang J 2017 *Mater. Horiz.* **4** 242
[27] Dominik K F and Gerasimos Konstantatos 2015 *Nano Lett.* **15** 7307
[28] Wang F, Mei J, Wang Y, Zhang L, Zhao H and Zhao D 2016 *ACS Appl. Mater. Interfaces* **8** 2840
[29] Li L, Huang Y, Peng J, Cao Y and Peng X 2014 *J. Mater. Chem. C* **2** 1372
[30] Lin Q, Armin A, Burn P L and Meredith P 2015 *Nat. Photon.* **9** 687
[31] Wang W, Zhao D, Zhang F, Li L, Du M, Wang C, Yu Y, Huang Q, Zhang M, Li L, Miao J, Lou Z, Shen G, Fang Y and Yan Y 2017 *Adv. Funct. Mater.* **27** 1703953
[32] Fang Y, Dong Q, Shao Y, Yuan Y and Huang J 2015 *Nat. Photon.* **9** 679
[33] Miao J, Zhang F, Lin Y, Wang W, Gao M, Li L, Zhang J and Zhan X 2016 *Adv. Opt. Mater.* **4** 1711
[34] He J, Luo M, Hu L, Zhou Y, Jiang S, Song H, Ye R, Chen J, Gao L and Tang J 2014 *J. Alloys Compd.* **596** 73
[35] Wang W, Zhang F, Du M, Li L, Zhang M, Wang K, Wang Y, Hu B, Fang Y and Huang J 2017 *Nano Lett.* **17** 1995
[36] Tian W, Zhou H and Li L 2017 *Small* **13** 1702107
[37] Zhong Y, Sisto T J, Zhang B, Miyata K, Zhu X Y, Steigerwald M L, Ng F and Nuckolls C 2017 *J. Am. Chem. Soc.* **139** 5644
[38] Bao C X, Chen Z L, Fang Y J, Wei H T, Deng Y H, Xiao X, Li L L and Huang J S 2017 *Adv. Mater.* **29** 1703209
[39] Rao H S, Li W G, Chen B X, Kuang D B and Su C Y 2017 *Adv. Mater.* **29** 1602639